

# Seeing All the Angles: Learning Multiview Manipulation Policies for Contact-Rich Tasks from Demonstrations

Trevor Ablett, Yifan Zhai, and Jonathan Kelly<sup>†</sup>

**Abstract**—Learned visuomotor policies have shown considerable success as an alternative to traditional, hand-crafted frameworks for robotic manipulation tasks. Surprisingly, the extension of these methods to the multiview domain is relatively unexplored. A successful multiview policy could be deployed on a mobile manipulation platform, allowing it to complete a task regardless of its view of the scene. In this work, we demonstrate that a multiview policy can be found through imitation learning by collecting data from a variety of viewpoints. We illustrate the general applicability of the method by learning to complete several challenging multi-stage and contact-rich tasks, from numerous viewpoints, both in a simulated environment and on a real mobile manipulation platform. Furthermore, we analyze our policies to determine the benefits of learning from multiview data compared to learning with data from a fixed perspective. We show that learning from multiview data has little, if any, penalty to performance for a fixed-view task compared to learning with an equivalent amount of fixed-view data. Finally, we examine the visual features learned by the multiview and fixed-view policies. Our results indicate that multiview policies implicitly learn to identify spatially correlated features with a degree of view-invariance.

## I. INTRODUCTION

The use of end-to-end visuomotor policies, in which observations are mapped directly to actions through a learned model, has emerged as an effective alternative to the traditional sense-plan-act approach for many robotic domains including autonomous vehicles [1], [2] and manipulators [3]–[6]. They are particularly appealing for manipulation, in which programming a robot to complete even relatively basic tasks can pose a major challenge.

Most research on learning end-to-end policies for manipulation, in which the input to the policy are easily-acquired camera images and proprioceptive sensor data, has focused on a fixed-base arm with a fixed viewpoint for the main imaging sensor. If these policies were naively rolled out in a task where the camera angle or base position changed even slightly, as would be the case for a mobile manipulator moving between tasks in an environment, one would not expect them to succeed since the network has no data corresponding to these changes. We seek to generate highly generalizable policies that are not brittle in the face of perturbations to the input, specifically, in this case, to changes in viewpoint.

All authors are with the Space & Terrestrial Autonomous Robotic Systems (STARS) Laboratory at the University of Toronto Institute for Aerospace Studies (UTIAS), Toronto, Canada <firstname>.<lastname>@robotics.utias.utoronto.ca.

<sup>†</sup>Jonathan Kelly is a Vector Institute Faculty Affiliate. This research was supported in part by the Canada Research Chairs program.

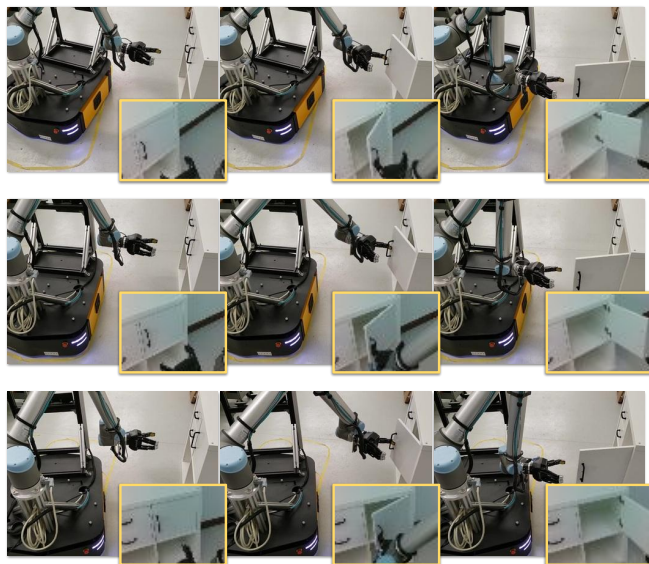


Fig. 1: Snapshots of three successful autonomous trajectories from different viewpoints in our real-world cabinet-opening task, executed by a single policy. The images in yellow boxes show the  $64 \times 48$  RGB sensor input to the policy used in this work, illustrating that the end-to-end policy has generalized to vastly different image data, as well as differing base poses, corresponding to each viewpoint.

In this work, we investigate the application of supervised imitation learning for generating end-to-end *multiview* policies for complex, contact-rich tasks. Specifically, we generate datasets containing trajectories with varying base poses, allowing policies to learn to complete tasks from a variety of viewpoints (see Fig. 1). Policies learned with this method can be directly applied to mobile manipulators in conjunction with a separate navigation policy that moves the mobile base to the vicinity of the manipulation task workspace [7].

Our contributions are answers to the following questions:

- 1) How does supervised imitation learning perform in a series of challenging multi-stage and contact-rich tasks in the multiview domain?
- 2) Will a policy trained with multiview data be penalized when performing an equivalent fixed-perspective task, compared to a policy trained with an equal amount of exclusively fixed-perspective data?
- 3) How far can fixed-base and multiview policies be pushed beyond their training distributions?
- 4) Compared with a fixed-view policy, do the features learned by a multiview policy show greater spatial correlation between different views?

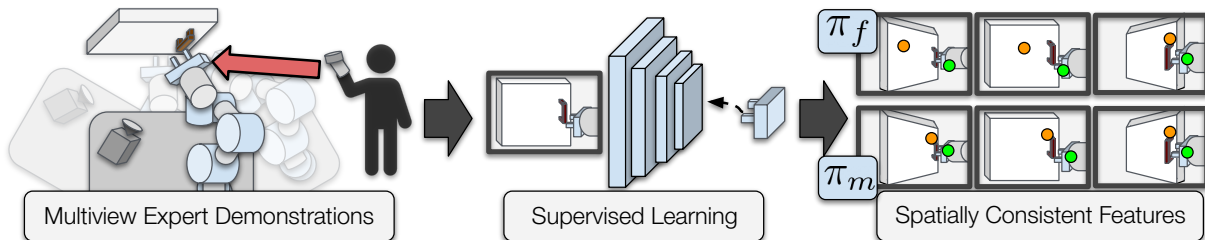


Fig. 2: Our system for generating multiview policies: after collecting expert demonstrations from numerous viewpoints, we train a deep neural network policy that generalizes to many views—further analysis shows that its features consistently label the same parts of objects.

Somewhat surprisingly, we demonstrate that multiview policies have near-equal performance to fixed-view policies in fixed-view domains, motivating their use in any case where a mobile base is present. In our work, we specifically do not add any explicit encoding of view-invariance in the loss function or policy architecture, and instead show that end-to-end multiview policies can be effectively trained implicitly by modifying the dataset.

## II. RELATED WORK

In this section, we begin by examining existing work on end-to-end policy learning for robotics, followed by learning-based mobile manipulation as well as other multiview manipulation work. We close with a brief discussion of supervised imitation learning, also known as behavior cloning.

The use of deep visuomotor policies to directly learn policies that map raw observations to actions for robotics has exploded in popularity recently, largely owing to representational power and generalization capabilities of deep neural networks and convolutional neural networks [3], [6], [8], [9]. Encoding a policy this way offers the advantage of being able to learn directly from data, given either expert actions or an external reward signal, without requiring the highly accurate world state information required for a traditional robotic framework based on the sense-plan-act paradigm. These policies have the downside of being limited to working with data that closely resembles the data they were trained on. In this work, we expand the training dataset to include multiple viewpoints, substantially improving the robustness of the learned policies.

Our approach can be compared to other learning-based methods being used for mobile manipulation. The system developed by [10] applies several learning techniques, combined with a graph-based connection between motion primitives, to complete several tasks. View-invariance of the control policies is encoded in separate object recognition and planning modules. Our method, in comparison, uses an end-to-end approach for completing tasks given raw sensor data only.

Several works have attempted to learn policies that control both a mobile base and a manipulator simultaneously, [11]–[13]. In each of these cases, the authors make assumptions about the availability of lower-level state information [11], [12], or the systems are only able to complete relatively simple reaching tasks [11], [13]. In our work, while we do not attempt to control the base during task execution,

we generate policies that can complete challenging, contact-rich tasks *without* access to privileged state information. The authors of [14] demonstrate a bed-making task using imitation learning and a mobile manipulator, driving the base to two specific locations to complete the task using fiducial markers for precise localization. Our method does not require explicit localization.

There has been some interest in learning policies that generalize to multiple views, even when a fixed-base manipulator is used. In one line of work, view synthesis has been applied to find models for generating arbitrary views, and prior work has shown that these simulated views [15] or their latent representations [16] can be used for generating higher-quality policies. This approach has two large drawbacks: it requires a potentially prohibitive amount of training data and operates on the assumption that all parts of images are equally relevant. In comparison, our method learns policies that output control signals given input images, ensuring that only the parts of the scene relevant for control are used.

In [17], the authors used a method based on domain randomization [18] to learn policies that were able to complete a multiview real-world reaching task by generating a large dataset of reaching data in simulation. The final policy is able to generalize to inputs from novel viewpoints. We attempt to complete tasks that require significantly higher dexterity than reaching alone.

Behavior cloning (BC) is the common name given to imitation learning treated as supervised learning [1], [19]: after collecting an expert dataset, a policy is trained to regress to expert actions given the corresponding observations. A core assumption of supervised learning is that the training data is independently and identically distributed (IID). In BC, this translates to assuming that the policy dataset, generated by running the policy, is drawn from the same distribution as the expert dataset. Unfortunately, in general this assumption is violated [20], but the problem can be mitigated by manually increasing the coverage of the expert dataset [1], [4], [5] or employing an intervention-based strategy [21]. We investigate the effects of including and excluding multiple views and base poses in the expert dataset for both multiview and fixed-base tasks.

## III. PROBLEM FORMULATION

We formulate our problem as a Markov Decision Process (MDP). Our goal is to learn a deterministic policy  $\pi_\theta : O \rightarrow A$ , parameterized by  $\theta$ , for environment observations  $o \in O$  and actions  $a \in A$ . Instead of maximizing a reward,

in imitation learning, we attempt to learn a task policy by matching a learned policy  $\pi_\theta$  to an expert policy  $\pi_E$ . In our case, we do not assume we have direct access to  $\pi_E$  and instead only have samples of human-generated demonstrations for a manipulation task  $\mathcal{D}_E := \{\tau_1, \dots, \tau_n, \dots, \tau_N\}$ ,  $\tau_n := \{(o_0, a_0), \dots, (o_t, a_t), \dots, (o_{T-1}, a_{T-1})\}$ , where  $T$  is the task horizon length. The initial observation  $o_0$  is sampled from an a priori defined distribution  $p(o_0)$ .

In this work, we train our policies using behavior cloning. A deterministic  $\pi_\theta$  can be trained by minimizing the mean squared error:

$$\min_{\theta} \sum_{(o,a) \in \mathcal{D}_E} (\pi_\theta(o) - a)^2. \quad (1)$$

In our work, each individual task or environment  $\mathcal{T}$  is a separate MDP that can be considered to be multiview  $\mathcal{T}_m$  or fixed-view  $\mathcal{T}_f$ , with  $\pi_m$  denoting a policy trained with data from  $\mathcal{T}_m$  (and  $\pi_f$  for  $\mathcal{T}_f$ ), where we omit  $\theta$  for convenience. For  $\mathcal{T}_f$ , we can define the observation generating process  $g_{O,f} : S_{\mathcal{M}} \times S_i \rightarrow O_{\mathcal{T}_f}$ , noting that  $o_{\mathcal{T}_f} \in O_{\mathcal{T}_f}$  are generated by an unknown function  $g_{O,f}$  of the underlying states of our manipulator  $s_{\mathcal{M}} \in S_{\mathcal{M}}$  and task relevant objects  $s_i \in S_i$ . The initial states of each episode  $s_{\mathcal{M},0}$  and  $s_{i,0}$  are uniformly randomized within predefined constraints. In contrast, we can define  $g_{O,m} : S_{\mathcal{M}} \times S_i \times S_b \rightarrow O_{\mathcal{T}_m}$ , where we have added the state of the base of our robot  $s_b \in S_b$ , noting that  $s_b$  is randomized between learning episodes only. In our formulation, measurements  $o \in O$  are acquired from a sensor attached to the robot base, so changing  $s_{b,0}$  affects  $s_{\mathcal{M},0}$ , the view of task relevant objects, and the set of actions that can solve the task.

#### IV. MULTIVIEW TRAINING AND SHARED INFORMATION

As stated in Section I, we are interested in the comparison between a multiview task  $\mathcal{T}_m$  and an equivalent fixed-base version  $\mathcal{T}_f$ , as well as policies  $\pi_m$  and  $\pi_f$  trained on observations  $O_{\mathcal{T}_m}$  and  $O_{\mathcal{T}_f}$ . It is important to note that because  $S_{\mathcal{M}}$  and  $S_i$  are shared between these environments and  $\dim(O_{\mathcal{T}_m}) = \dim(O_{\mathcal{T}_f})$ , we can generate actions from  $\pi_m$  or  $\pi_f$  with both  $O_{\mathcal{T}_m}$  and  $O_{\mathcal{T}_f}$ .

##### A. Comparing $\mathcal{T}_m$ and $\mathcal{T}_f$

Considering the sizes of the sets of possible states for  $\mathcal{T}_m$  and  $\mathcal{T}_f$  leads to a well-known challenge in prediction problems that is related to the curse of dimensionality [22]: since  $\dim(S_{\mathcal{M}} \times S_i \times S_b) > \dim(S_{\mathcal{M}} \times S_i)$ , we should require significantly more training examples from  $O_{\mathcal{T}_m}$  to learn  $\pi_m$  than from  $O_{\mathcal{T}_f}$  to learn  $\pi_f$  (i.e., to achieve the same success rate). Said differently, more examples are required to adequately ‘cover the space’  $O_{\mathcal{T}_m}$  than to cover  $O_{\mathcal{T}_f}$ .

A natural conclusion is that, given the same quantity of training data,  $\pi_m$  will perform *worse* than  $\pi_f$  on  $\mathcal{T}_f$ , for two separate but related reasons: i)  $\pi_m$  is required to learn a higher-dimensional problem than  $\pi_f$ , and ii)  $\pi_m$  is provided with less (or possibly no)  $o_{\mathcal{T}_f} \in O_{\mathcal{T}_f}$  at training time.

##### B. When Multiview Data Helps

Implicit in the above conclusion is the assumption that, for a specific task, the distributions of expert actions  $p(a_E | s_b = \alpha)$  and  $p(a_E | s_b = \beta)$  for two different base poses,  $\alpha, \beta \in S_b$ , are independent. However, this is not true for our problem, or for many other supervised learning tasks—the distributions of observations, and actions, for poses that are ‘nearby’ in the state space,  $S_b$ , must have nonzero mutual information.<sup>1</sup> If this were not the case, multiview policies would be unable to generalize to new poses. We experimentally show that our policies are able generalize to new poses (in Section VII-A) and also to out-of-distribution data (in Section VII-B). We consider the task-dependent mutual information  $I(A_{E,\alpha}; A_{E,\beta})$  between  $A_{E,\alpha} \sim p(a_E | s_b = \alpha)$  and  $A_{E,\beta} \sim p(a_E | s_b = \beta)$  below.

For tasks where  $I(A_{E,\alpha}; A_{E,\beta})$  is large in general,  $\pi_m$  will provide little benefit over  $\pi_f$  in  $\mathcal{T}_m$ . However, when  $I(A_{E,\alpha}; A_{E,\beta})$  is small in general,  $\pi_m$  may be prohibitively costly to learn and suffer compared with  $\pi_f$  in  $\mathcal{T}_f$ . This issue arises due to the increased number of expert demonstrations needed to cover the space of  $O_{\mathcal{T}_m}$ . For this reason, we expect  $\pi_m$  will provide the most benefit, compared to  $\pi_f$  learned from an equivalent amount of data, when  $I(A_{E,\alpha}; A_{E,\beta})$  falls somewhere in the middle—each base pose generates similar observations and requires a similar, but not identical, trajectory of actions to allow successful completion of the task (see Fig. 1). As an example, consider a lifting task, where the robot has to lift an object sitting on a table. If, when varying  $s_b$ , the object poses in the set  $S_{i,0}$  remain the same relative to both the imaging sensor and the robot base, a multiview policy would provide little benefit. Conversely, consider a door opening task, where the robot has to open a cabinet door: the initial pose of the cabinet  $s_{i,0}$  does not change relative to the world. Therefore, if  $s_b$  is changed, the initial pose of the cabinet, relative to the imaging sensor and the robot base, will necessarily change, and a fixed-view policy will likely fail.

We can rephrase one of our primary experimental questions as follows: provided a task has an upper bound on the range of base poses to consider, is there sufficient mutual information between trajectories at different (but ‘nearby’) poses to enable a policy  $\pi_m$  to be learned that not only performs adequately in  $\mathcal{T}_m$ , but performs comparably to  $\pi_f$  in  $\mathcal{T}_f$ , given the same amount of training data? That is, if we reduce the sampling density (of expert demonstrations), is the mutual information between those demonstrations sufficient to ensure that  $\pi_m$  performs well in  $\mathcal{T}_m$  and similarly to  $\pi_f$  in  $\mathcal{T}_f$ ? We examine this question in Section VII-A.

Finally, despite nonzero mutual information, it remains true that  $\pi_m$  must learn in the larger ‘space’ of  $O_{\mathcal{T}_m}$ , compared to  $\pi_f$  and  $O_{\mathcal{T}_f}$ . If  $\pi_m$  relies on mutual information, we would expect that many of the visual features learned by  $\pi_m$  would consistently refer to the same parts of the scene, regardless of viewpoint, a possibility which we examine in

<sup>1</sup>This condition depends upon another assumption, of smoothness of the state, observation, and action spaces.



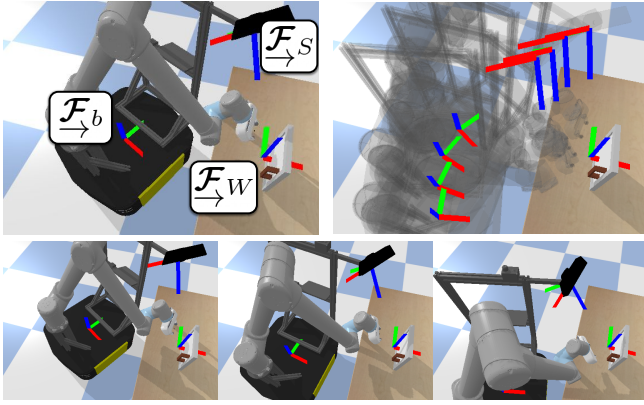


Fig. 3: Top left: Relevant robot and task reference frames. Top right: A set of four base poses, shown to illustrate the semi-circle of possible poses. Bottom: Base poses where  $b_\phi$  is set to  $b_{\phi,\min}$ ,  $0.5(b_{\phi,\min} + b_{\phi,\max})$ , and  $b_{\phi,\max}$ .

### Section VII-C.

## V. METHODOLOGY

### A. Choosing New Views

As previously noted, we assume that we have access to an “approach” policy that is capable of moving the mobile base to a pose where the task-relevant objects are both a) in view of the base-mounted sensor and b) within the reachable workspace of the manipulator.

We use an automated process to generate randomized base poses for each new training process. We require a) a rough estimate of the transform from the robot base frame to the sensor, b) a rough estimate of the robot base pose in the fixed workspace (i.e., world) reference frame (the estimate from wheel odometry is adequate), c) a pre-selected centre point in the workspace frame, and iv) the desired distance (again, approximate) between the camera frame origin and the centre point in the workspace frame. Our goal is to solve for poses of the mobile base that ensure that the main optical axis of the camera sensor, at  $\mathcal{F}_S$ , always very nearly intersects with the selected centre point in the workspace frame at  $\mathcal{F}_W$ —each pose in the feasible set lies on a circle, as shown in Fig. 3. Since the base poses are in  $SE(2)$ , they can be defined by  $b_\phi, b_x$  and  $b_y$ : new poses are generated by randomly sampling  $b_\phi \sim U(b_{\phi,\min}, b_{\phi,\max})$  (where  $b_{\phi,\min}$  and  $b_{\phi,\max}$  are set to ensure that there are no collisions with the environment) and computing the appropriate corresponding  $b_x$  and  $b_y$  using the constraints outlined above. After sampling and solving for the full base pose, we add a small amount of uniform random noise to the pose values, with the aim of increasing the robustness of our learned policy. Care must be taken to ensure that, when random noise is added, the task-relevant objects remain within the field of view of the camera and within the reachable operational space of the manipulator.

Importantly, our learned policies do not require direct knowledge of the base-to-camera transform or the workspace-to-base transform—this information is used only during the autonomous view generation process. In general, assuming that the learned policies have access to accurate

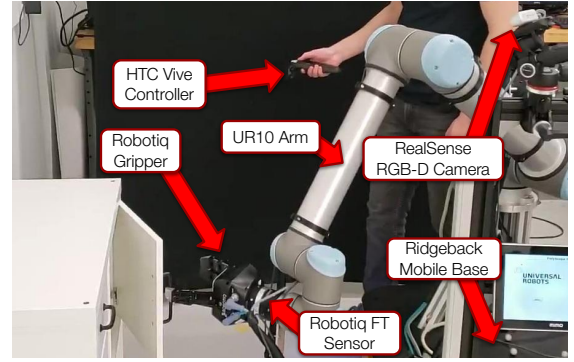


Fig. 4: Our experimental setup in the real world. Pictured is our mobile manipulation platform as described in Section VI-A, as well as a human demonstrator in the process of collecting a demonstration for our *DoorReal* task.

estimates of the transform parameters would introduce substantial limitations.

### B. Collecting Human Expert Data

Our method requires the collection of a dataset  $\mathcal{D}_E$  of expert trajectories of observation-action pairs  $(o, a)$  acquired through teleoperation. We only require that the demonstrations are collected without an operator in view of the imaging sensor, though we note that this constraint exists for all imitation learning methods that generate visuomotor policies.

## VI. EXPERIMENTAL SETUP

### A. Hardware

We complete experiments on both simulated and real versions of our mobile manipulation platform: a UR10 robotic arm mounted on a Clearpath Ridgeback omnidirectional base, as shown in Fig. 4. Our real platform has a Robotiq 3-finger gripper, while our simulated platform in PyBullet [23] uses either a PR2 gripper or a Franka Emika Panda gripper (either of which is easier to simulate than the 3-finger gripper).

On our physical platform, we employ a simple compliant controller using a Robotiq FT-300 force-torque sensor, allowing our policies, all of which require significant contact with the environment, to operate safely. Using a compliant controller has been shown in previous work [24] to be an effective way to use a learned policy for completing contact-rich tasks. Our robot is controlled using off-the-shelf ROS packages at the lower-level and our own inverse kinematics (IK) library.

On both the real and the simulated platforms, we use RGB and depth images as inputs to our policies. On the real platform, images are generated using a RealSense D435, and aligned using the official ROS library provided by Intel. The sensor is firmly mounted to the sensor mast attached to the mobile base (see Fig. 4), ensuring that, when the base moves, the sensor moves with it (see Fig. 3).

To collect human demonstrations, we use a single HTC Vive hand controller (see Fig. 4) and custom-designed software. For visual feedback, we found that having the user observe the real robot during collection was sufficient. We

TABLE I: Environments used in this work. Demo time is the cumulative real time of the 200 demonstrations in the multiview version each expert dataset and the  $p(o_0)$  params are the initial conditions of the environment that are randomized between episodes. The “base  $b_\phi$  range” corresponds to  $b_{\phi, \max} - b_{\phi, \min}$ , as described in Section V-A.

Environment	Objective	Demo time	$p(o_0)$ params	$p(o_0)$ (ranges)	Actions
<i>LiftSim</i>	Reach block and lift above 7.5cm	18m23s	base pose, block pose	base $b_\phi$ range: $45^\circ$ , block center in $25\text{cm} \times 25\text{cm}$ box	Trans vel, grip
<i>StackSim</i>	Stack blue block on green block	25m05s	base pose, blue block pose, green block pose	base $b_\phi$ range: $45^\circ$ , block centers in $15\text{cm} \times 15\text{cm}$ box	6-DOF vel, grip
<i>PickAndInsertSim</i>	Grasp cylinder and insert in hole ( $<1\text{mm}$ tol.)	14m23s	base pose, cylinder pose	base $b_\phi$ range: $45^\circ$ , cylinder center in $2.5\text{cm} \times 2.5\text{cm}$ box	6-DOF vel, grip
<i>DoorSim</i>	Grasp door handle, open $>90^\circ$	25m17s	base pose, initial gripper pose	base $b_\phi$ range: $45^\circ$ , gripper: in $12\text{cm} \times 5\text{cm} \times 5\text{cm}$ box	6-DOF vel, grip
<i>PickAndInsertReal</i>	Grasp cylinder and insert in hole ( $<1\text{mm}$ tol.)	28m30s	base pose, cylinder pose	base $b_\phi$ range: $35^\circ$ , cylinder center in $2.5\text{cm} \times 2.5\text{cm}$ box	6-DOF vel, grip
<i>DoorReal</i>	Hook door handle, open $>90^\circ$	30m56s	base pose, initial gripper pose	base $b_\phi$ range: $35^\circ$ , gripper: in $12\text{cm} \times 5\text{cm} \times 5\text{cm}$ box	6-DOF vel
<i>DrawerReal</i>	Hook drawer handle, open within 2cm of max	32m23s	base pose, initial gripper pose	base $b_\phi$ range: $35^\circ$ , gripper: in $12\text{cm} \times 5\text{cm} \times 5\text{cm}$ box	6-DOF vel

also use the force-torque sensor to provide proportional haptic feedback to the demonstrator through the vibration motor in the controller—the vibration amplitude increases with the norm of the force and/or torque.

### B. Environments

For a summary of our environments/tasks, see Table I. Representative images from successful trajectories in each environment are shown in Fig. 5. All of the tasks’ input data include, in addition to RGB and depth images, the current pose of the end-effector in the frame of the robot, provided

by forward kinematics and represented as a 7-tuple with position and a unit quaternion for orientation. As well, each task that requires actuating the gripper includes the current and previous two positions of each gripper finger. Finally, the real environments also include data from the force-torque sensor.

### C. Policy Architecture and Training

Our policies use a similar architecture to [4]. Specifically, we use a mutli-layer convolutional neural network (CNN) to process the RGB and depth images, take the spatial softmax [3] of the final CNN layer, and concatenate those points with other numerical state information before pushing them through a set of two fully-connected layers. Our CNN layers are the same as in [4], but we use 512 neurons in each of our fully-connected hidden layers. Crucially, all input is available from raw sensor data, and our policy does not have access to any privileged state information, including object poses or the relative base pose. We reduce the resolution of our RGB and depth images to  $64 \times 48 \times 3$  and  $64 \times 48$ , respectively, and initialize the weights of the RGB layer with weights from ResNet [25]. Empirically we found greatly reduced variance between the performance of differently-seeded policies by training our policies as ensembles [26], so each policy is a five-member ensemble, with the final output being the mean output. Each member policy is trained with the same data shuffled differently, with member weights being initialized with different random orthogonal weights (apart from the pretrained weights).

We train the policies using Tensorflow [27] and the Adam optimizer [28] with early stopping, ending training when the validation error on a 20% holdout set has not improved for 30 epochs. We use a learning rate of 0.001, a mini-batch size of 64, and a maximum of 200 epochs. Our loss function is the mean squared error (Eq. (1)) between the expert and policy action—we do not use the auxiliary losses from [4].

The *LiftSim* environment policies are trained using demonstrations generated from a policy learned with Soft-Actor Critic [29] to encourage repeatable experiments. Given the high cost of generating autonomous policies for the other tasks, all other tasks use exclusively human-generated data.

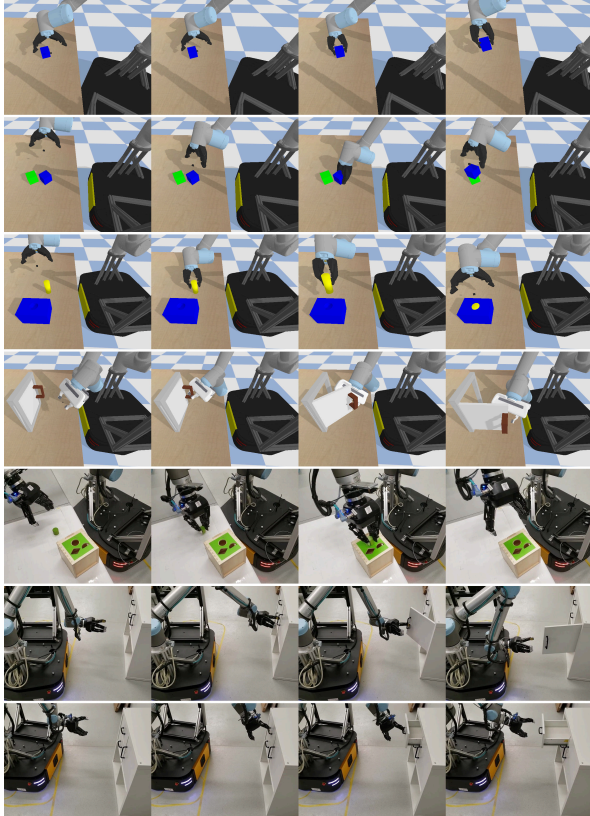


Fig. 5: Successful trajectories for tasks studied in this work. From top to bottom: *LiftSim*, *StackSim*, *PickAndInsertSim*, *DoorSim*, *PickAndInsertReal*, *DoorReal*, and *DrawerReal*.

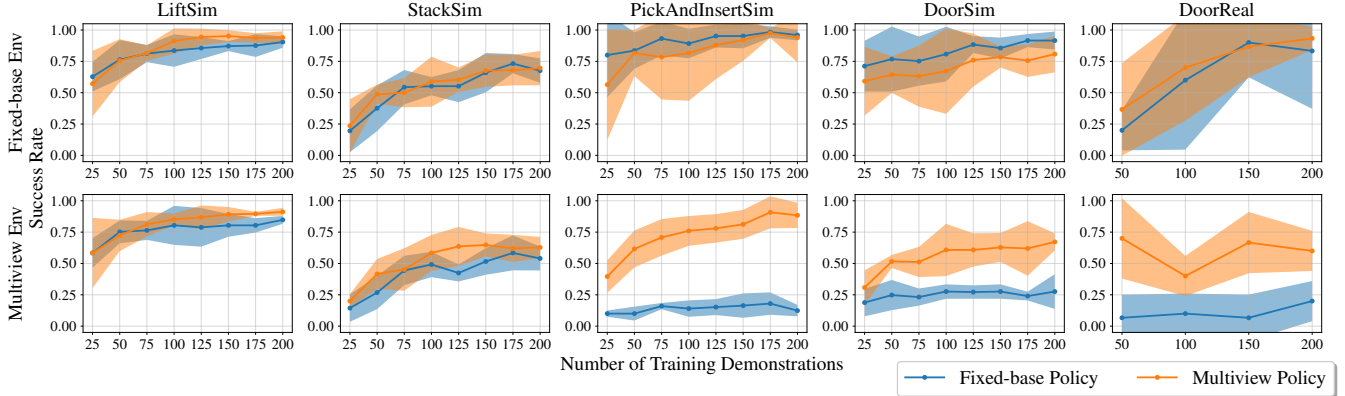


Fig. 6: Performance of our policies in environments in which we compared fixed-base with multiview policies in fixed-base (top) and multiview (bottom) environments. The shaded region shows the two-sigma bounds across five policy seeds in simulation environments, and three in *DoorReal*. The multiview policies, as expected, outperform fixed-base policies in multiview settings, often substantially so, with either no or only minor detriment compared with a fixed-base policy in a fixed-base environment.

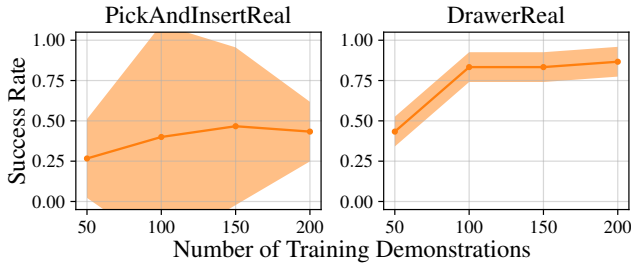


Fig. 7: Performance results for other real environments in which we only tested multiview policies. The shaded region shows the two-sigma bounds across three policy seeds.

## VII. EXPERIMENTAL RESULTS

Our goal in this work is to investigate the performance of multiview policies relative to fixed-view policies on a series of contact-rich manipulation tasks. To do so, we compare the performance of  $\pi_m$  and  $\pi_f$  in both  $\mathcal{T}_m$  and  $\mathcal{T}_f$  and on out-of-distribution data. To attempt to explain performance gaps, we additionally examine the spatial consistency of the features learned by  $\pi_m$  and  $\pi_f$ .

For each task, we collected 200 demonstrations and trained five policies, with different seeds and at multiple demonstration quantities, and finally ran a series of test episodes with held-out initial conditions to evaluate the success rate of each policy. We trained our policies with increments of 25 demonstrations/50 episodes per policy and 50 demonstrations/10 episodes per policy, in simulation and on the real robot, respectively.

### A. Multiview versus Fixed-base

For *LiftSim*, *StackSim*, *PickAndInsertSim*, *DoorSim*, and *DoorReal*, we collected both multiview and fixed-base data on each task, and compared performance under four conditions:  $\pi_m$  in  $\mathcal{T}_m$ ,  $\pi_m$  in  $\mathcal{T}_f$ ,  $\pi_f$  in  $\mathcal{T}_m$ , and  $\pi_f$  in  $\mathcal{T}_f$  (see Fig. 6). Notably, as we predicted in Section IV-B, in the Lift and Stack environments, the multiview policy only provides a marginal benefit over a fixed-base policy in a multiview environment. For these two environments, the  $\pi_m$  does not perform any worse than  $\pi_f$  in  $\mathcal{T}_f$ , indicating that

a multiview policy can improve performance, and does not appear to cause any detriment.

The benefits of a multiview policy are much clearer in the *PickAndInsertSim*, *DoorSim*, and *DoorReal* environments, where the fixed-base policy fails often in the multiview case, while the multiview policy, as expected, increases in performance with the number of demonstrations. Compared with a fixed-base policy, the multiview policy does lose a small amount of performance in the  $\mathcal{T}_f$  *DoorSim* task. Notably, we do not see the same effect in the real world version of the Door task—we suspect that in the real world, it is quite difficult to ensure that the base is in the *exact* same pose it was in during data collection. Of course, this small deviation is not an issue for the multiview policy and further motivates its use over a fixed-view policy.

The performance results of multiview policies for *PickAndInsertReal* and *DrawerReal* are shown in Fig. 7. As is the case for *PickAndInsertSim*, *DoorSim*, and *DoorReal*, we would reasonably expect that a fixed-base policy would not be able to complete these tasks successfully given differing views. It is worth noting that the performance variation between differently-seeded policies for *PickAndInsertReal* is relatively high. We suspect this is due to the difficulty of learning this task in a purely supervised framework—empirically, many of the failures in this environment were “near-misses,” in which the cylindrical block only *just* missed being inserted.

### B. Out-of-Distribution (OOD) Experiments

To investigate performance on OOD data, we compared the performance of multiview policies with fixed-view policies given specific base angles,  $b_\phi$ , as described in Section V-A. Our multiview policies were trained in our simulated environments with  $b_\phi \sim U(-0.6, 0.2)$  (radians), and our fixed-view policies were trained with  $b_\phi = 0$ . We test both policies with 12 sets of initial conditions for  $b_\phi$ :  $b_{\phi, \text{range}} = \{[-0.8, -0.7], [-0.7, -0.6], \dots, [0.3, 0.4]\}$ . We draw 50 random values from each  $b_{\phi, \text{range}}$ , and record the success rate on these episodes for five seeds of multiview



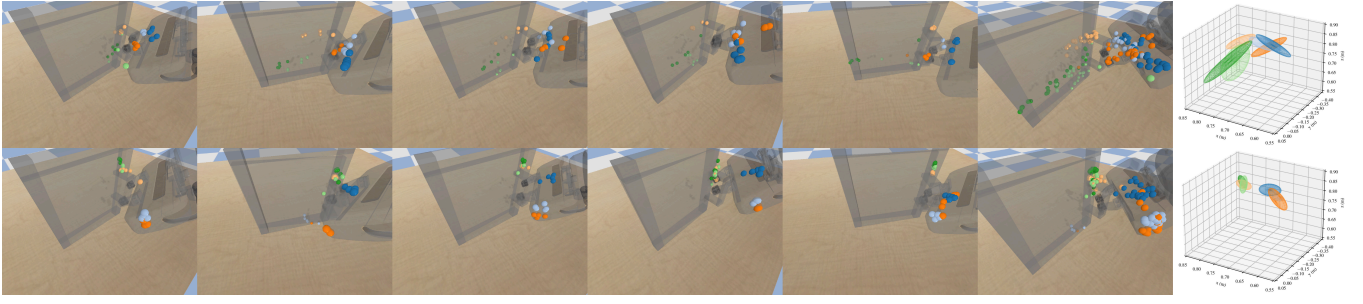


Fig. 8: A comparison of the three SSAM points with highest activation on the gripper and the door, reprojected from five different time steps for five different episodes with different viewpoints. The first five images of each row show the locations of the six features for each different viewpoint and the sixth image shows all SSAM points reprojected to a single view. The features in the top diagrams are from  $\pi_f$ , and display far less spatial consistency than the features in the bottom diagrams from  $\pi_m$ . The ellipsoids on the right show the two-sigma bounds of the covariance of all of the object-consistent SSAM positions. Each SSAM output corresponds to a different colour.

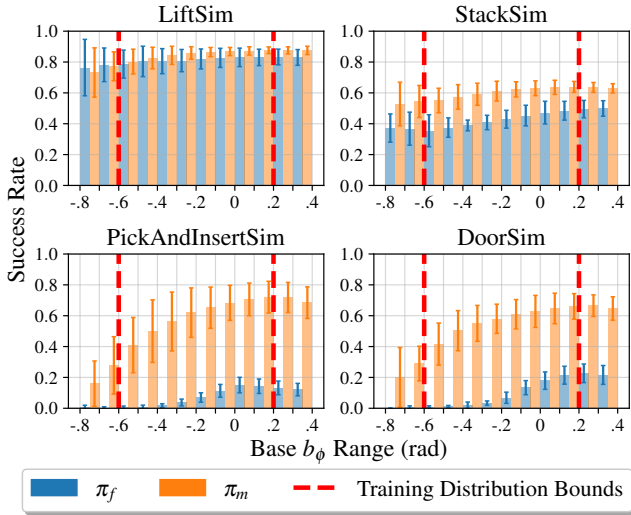


Fig. 9: Results of testing multiview policies ( $\pi_m$ ) and fixed-base policies ( $\pi_f$ ), each trained with 200 demonstrations, in multiview environments at a range of angles. The whiskers show the two-sigma bounds across five policy seeds. Here,  $\pi_m$  outperforms  $\pi_f$ , and also shows some ability to perform adequately outside of the training distribution bounds.

policies and fixed-base policies, each trained with 200 expert demonstrations. The results are shown in Fig. 9.

As predicted, both types of policies tend to perform roughly equally in each range of angles in *LiftSim*, and, as described in Section VII-A, the *StackSim* multiview policy tends to perform better in general. For *PickAndInsertSim* and *DoorSim*, a clearer picture emerges to explain the performance difference shown in Fig. 6: the fixed-base policies were trained exclusively at  $b_\phi = 0$  with no variation in  $b_x$  or  $b_y$ , so  $\pi_f$  performance, with even small variations in  $b_\phi$ , falls dramatically compared with the performance of  $\pi_f$  on  $\mathcal{T}_f$ . The performance of  $\pi_f$  continues to deteriorate as  $|b_\phi|$  increases, while the multiview policies do well throughout the training distribution, with a noticeable negative skew in performance towards the negative angles. The reduced performance may occur because our camera is already at an angle to the left of the scene (see Fig. 3), so moving it further to the left makes the task particularly challenging. The multiview policies show some degree of ability to generalize beyond their training distribution, indicating that

the multiview policies learn at least some information about the geometric relationship between the arm and the objects in the scene, regardless of the viewpoint.

### C. Learned Feature Analysis

Expanding on our analysis in Section IV-B, we compare the visual features learned by policies  $\pi_f$  and  $\pi_m$ . The vision portion of our network terminates with a set of 32 spatial soft-argmax (SSAM) outputs per ensemble member, generated from each of the last convolutional filters, which can be interpreted as points in image space (we refer the reader to [3] for a more detailed explanation of SSAM). In this section, we refer to SSAM outputs/points interchangeably as features, but unlike traditional features in computer vision (i.e., those used for feature matching), they do not specifically encode a descriptor that can consistently identify the same parts of different images.

The use of SSAM outputs allows us to interpret where the network directs its attention. We can therefore observe whether individual SSAM outputs are spatially consistent, which would imply that a view-independent geometric representation has been learned and potentially (partially) explain generalization capability. As noted in Section IV-B, the reuse of information between views would lead to spatially consistent (correlated) features.

For this analysis, we used five random episodes (i.e., with five different views) of each of  $\pi_m$  and  $\pi_f$  acting in  $\mathcal{T}_m$  in our *DoorSim* environment. In each episode, starting from one time step before the policy initially closed the gripper (attempting to grasp the door handle—arguably the most challenging part of the task), we recorded all of the SSAM points and activation magnitudes from each policy for five time steps. These SSAM points were then projected into Cartesian space using the known camera intrinsic parameters, depth image data, and the world gripper and door poses. Given five episodes and five time steps, each SSAM output produces 25 3D feature points in the world frame. We sorted the SSAM points by their activation magnitudes, and took the three SSAM points with the highest average activation magnitudes that also showed up at least 20 out of 25 times on either the door or the gripper (as determined using ground-truth information from PyBullet), yielding six representative SSAM outputs in total for each of  $\pi_m$  and  $\pi_f$ . Each of these

six SSAM features had (up to) 25 positions on either the gripper or the door. We plotted the reprojected locations of these features in Fig. 8 (with features from  $\pi_f$  on the top row and from  $\pi_m$  on the bottom row).

The features learned by  $\pi_m$  clearly show a smaller degree of spread, and therefore higher spatial correlation, than the features from  $\pi_f$ . The spatial correlation of the SSAM layer activations indicates that a degree of view-invariance has been learned without the need to explicitly train using a view-invariance loss or architecture—the policy has learned a visual representation of the task-relevant objects (including the arm) in terms of features that are robust to viewpoint changes. Our interpretation that  $\pi_m$  has learned a degree of true view-invariance is also supported by our results in Section VII-B:  $\pi_m$  generalizes (without major penalties in performance) to large viewpoint shifts *beyond* its training distribution.

## VIII. CONCLUSION AND FUTURE WORK

In this paper, we generated end-to-end policies for challenging, contact-rich tasks involving multiple views. We demonstrated the benefits of multiview policies through extensive experiments on a mobile manipulation platform in both simulation and the real world. Specifically, given the same amount of training data, a multiview policy can be learned with very little, if any, detriment to performance compared with a fixed-base policy and a corresponding fixed-base task. Since multiview policies are considerably more flexible than their fixed-based counterparts, we assert that multiview data is potentially always desirable. As future work, we would like to further investigate methods for reducing the data required to learn effective policies through the use of traditional and learning-based view synthesis techniques.

## REFERENCES

- [1] D. A. Pomerleau, “ALVINN: An Autonomous Land Vehicle in a Neural Network,” in *Proc. Ann. Conf. Neural Information Processing Systems (NIPS’89)*, D. S. Touretzky, Ed., 1989, pp. 305–313.
- [2] M. Bojarski, *et al.*, “End to End Learning for Self-Driving Cars,” *arXiv:1604.07316 [cs]*, Apr. 2016.
- [3] S. Levine, C. Finn, T. Darrell, and P. Abbeel, “End-to-End Training of Deep Visuomotor Policies,” *J. Machine Learning Research*, vol. 17, no. 39, pp. 1–40, 2016.
- [4] T. Zhang, *et al.*, “Deep Imitation Learning for Complex Manipulation Tasks from Virtual Reality Teleoperation,” in *Proc. IEEE Int. Conf. Robotics and Automation (ICRA’18)*, May 2018, pp. 5628–5635.
- [5] M. Laskey, J. Lee, R. Fox, A. D. Dragan, and K. Goldberg, “DART: Noise Injection for Robust Imitation Learning,” in *Proc. 1st Ann. Conf. Robot Learning (CoRL’17)*, Nov. 2017, pp. 143–156.
- [6] R. Rahmatizadeh, P. Abolghasemi, L. Boloni, and S. Levine, “Vision-Based Multi-Task Manipulation for Inexpensive Robots Using End-to-End Learning from Demonstration,” in *Proc. IEEE Int. Conf. Robotics and Automation (ICRA’18)*, May 2018, pp. 3758–3765.
- [7] A. Iriondo, E. Lazkano, L. Susperregi, J. Uraín, A. Fernandez, and J. Molina, “Pick and Place Operations in Logistics Using a Mobile Manipulator Controlled with Deep Reinforcement Learning,” *Applied Sciences*, vol. 9, no. 2, p. 348, Jan. 2019.
- [8] C. Finn, S. Levine, and P. Abbeel, “Guided Cost Learning: Deep Inverse Optimal Control via Policy Optimization,” in *Proc. 33rd Int. Conf. Machine Learning (ICML’16)*, ser. ICML’16, June 2016, pp. 49–58.
- [9] F. Codevilla, M. Müller, A. López, V. Koltun, and A. Dosovitskiy, “End-to-End Driving Via Conditional Imitation Learning,” in *Proc. IEEE Int. Conf. Robotics and Automation (ICRA’18)*, May 2018, pp. 4693–4700.
- [10] M. Bajracharya, *et al.*, “A Mobile Manipulation System for One-Shot Teaching of Complex Tasks in Homes,” in *Proc. IEEE Int. Conf. Robotics and Automation (ICRA’20)*, May 2020, pp. 11 039–11 045.
- [11] C. Wang, *et al.*, “Learning Mobile Manipulation through Deep Reinforcement Learning,” *Sensors (Basel, Switzerland)*, vol. 20, no. 3, Feb. 2020.
- [12] T. Welschehold, C. Dornhege, and W. Burgard, “Learning Mobile Manipulation Actions from Human Demonstrations,” in *Proc. IEEE/RSJ Int. Conf. Intelligent Robots and Systems (IROS’17)*, Sep. 2017, pp. 3196–3201.
- [13] J. Kindle, F. Furrer, T. Novkovic, J. J. Chung, R. Siegwart, and J. Nieto, “Whole-Body Control of a Mobile Manipulator Using End-to-End Reinforcement Learning,” *arXiv:2003.02637 [cs]*, Feb. 2020.
- [14] M. Laskey, C. Powers, R. Joshi, A. Poursohi, and K. Goldberg, “Learning Robust Bed Making Using Deep Imitation Learning with DART,” *arXiv:1711.02525 [cs]*, Nov. 2017.
- [15] A. Amini, *et al.*, “Learning Robust Control Policies for End-to-End Autonomous Driving From Data-Driven Simulation,” *IEEE Robotics and Automation Letters*, vol. 5, no. 2, pp. 1143–1150, Apr. 2020.
- [16] S. M. A. Eslami, *et al.*, “Neural Scene Representation and Rendering,” *Science*, vol. 360, no. 6394, pp. 1204–1210, June 2018.
- [17] F. Sadeghi, A. Toshev, E. Jang, and S. Levine, “Sim2Real Viewpoint Invariant Visual Servoing by Recurrent Control,” in *Proc. IEEE/CVF Conf. Computer Vision and Pattern Recognition (CVPR’18)*, June 2018, pp. 4691–4699.
- [18] J. Tobin, R. Fong, A. Ray, J. Schneider, W. Zaremba, and P. Abbeel, “Domain Randomization for Transferring Deep Neural Networks from Simulation to the Real World,” in *Proc. IEEE/RSJ Int. Conf. Intelligent Robots and Systems (IROS’17)*, Sep. 2017, pp. 23–30.
- [19] M. Bain and C. Sammut, “A Framework for Behavioural Cloning,” in *Machine Intelligence 15*, 1996, pp. 103–129.
- [20] S. Ross, G. J. Gordon, and D. Bagnell, “A Reduction of Imitation Learning and Structured Prediction to No-Regret Online Learning,” in *Proc. 14th Int. Conf. Artificial Intelligence and Statistics (AISTATS’11)*, 2011, pp. 627–635.
- [21] T. Ablett, F. Marić, and J. Kelly, “Fighting Failures with FIRE: Failure Identification to Reduce Expert Burden in Intervention-Based Learning,” *arXiv:2007.00245 [cs]*, Aug. 2020.
- [22] R. Bellman, *Dynamic Programming*, ser. Dover Books on Computer Science Series, 1957.
- [23] E. Coumans and Y. Bai, “PyBullet, a Python Module for Physics Simulation for Games, Robotics and Machine Learning,” 2016.
- [24] M. A. Lee, *et al.*, “Making Sense of Vision and Touch: Self-Supervised Learning of Multimodal Representations for Contact-Rich Tasks,” in *Proc. IEEE Int. Conf. Robotics and Automation (ICRA’19)*, May 2019, pp. 8943–8950.
- [25] K. He, X. Zhang, S. Ren, and J. Sun, “Deep Residual Learning for Image Recognition,” in *Proc. IEEE Conf. Computer Vision and Pattern Recognition (CVPR’16)*, June 2016, pp. 770–778.
- [26] L. Breiman, “Bagging Predictors,” *Machine Learning*, vol. 24, no. 2, pp. 123–140, Aug. 1996.
- [27] M. Abadi, *et al.*, “TensorFlow: Large-Scale Machine Learning on Heterogeneous Systems,” 2015.
- [28] D. P. Kingma and J. Ba, “Adam: A Method for Stochastic Optimization,” in *Proc. Int. Conf. Learning Representations (ICLR’15)*, May 2015.
- [29] T. Haarnoja, A. Zhou, P. Abbeel, and S. Levine, “Soft Actor-Critic: Off-Policy Maximum Entropy Deep Reinforcement Learning with a Stochastic Actor,” in *Proc. 35th Int. Conf. Machine Learning (ICML’18)*, July 2018, pp. 1861–1870.